

Geometric and Mechanical Characterization of Human Carpal Bones – a Preliminary Study

Dénes Faragó^{1,2}, Rita M. Kiss^{1,2*}

¹ Cooperation Research Center for Biomechanics, Faculty of Mechanical Engineering, Budapest University of Technology and Economics, Budapest, Hungary , 1111 Budapest, Műegyetem rkp. 3.

² Department of Mechatronics, Optics and Mechanical Engineering Informatics, Faculty of Mechanical Engineering, Budapest University of Technology and Economics, Budapest, Hungary, 1111 Budapest, Műegyetem rkp. 3

* Corresponding author, e-mail: rita.kiss@mogi.bme.hu

Received: 15 October 2019, Accepted: 21 October 2019, Published online: 15 January 2020

Abstract

Human hand injuries account for a significant number of accidents of young adults (mostly sports injuries) and elderly people. The most vulnerable part of the hand is the wrist, a construct consisting of numerous bones and ligaments. The hand is a complex structure, the mechanical behavior is hard to describe, and also it is sometimes hard to correctly diagnose the injuries. The goal of the present research is to create a quickly and inexpensive measurement method to characterize the geometrical and mechanical properties of carpal bones.

The method presented is suitable to properly characterize the intact and damaged geometries of different carpal bones (capitate scaphoid, trapezium, pisiform). 3D models of intact and failed bones are determined by a 3D scanner, mechanical properties are determined with high-speed compression load (700 mm/min), which represents the fracture by falling down.

According to the test results, the 3D scanning technique provided valuable geometrical data for cross-section calculation (scan before the test) and for analysis of the failure mode of the bones (scan after the test). The modulus of elasticity data for finite element simulation can be determined by the high-speed compression tests.

Keywords

human hand, carpal bones, carpal tunnel, mechanical test, 3D image

1 Introduction

Characterizing the mechanical properties of bone and tissues is fundamental for advances in numerous areas of biomedicine such as diagnostics, forensics, surgical simulations, and injury prediction [1–5]. Various methods have been used to determine the properties of tissues such as tension testing, compression testing, perfusion, probing, aspiration, and imaging [1, 3, 6–8].

The human hand is often exposed to injury, it dampens falls, raises hard things, but it can also be damaged during sports and play. One of the most important parts of the hand is the wrist, consisting of 8 bones: capitate (os Capitatum), lunate (os lunatum), triquetrum (os triquetrum), pisiform (os pisiforme), scaphoid (os scaphoid), trapezium (os trapezioidum), pisiform (os capitatum) and hamate (os hamatum). The carpal bones are bounded by the radius and the ulna from the arm, the fingers and the metacarpale (Fig. 1) [9].

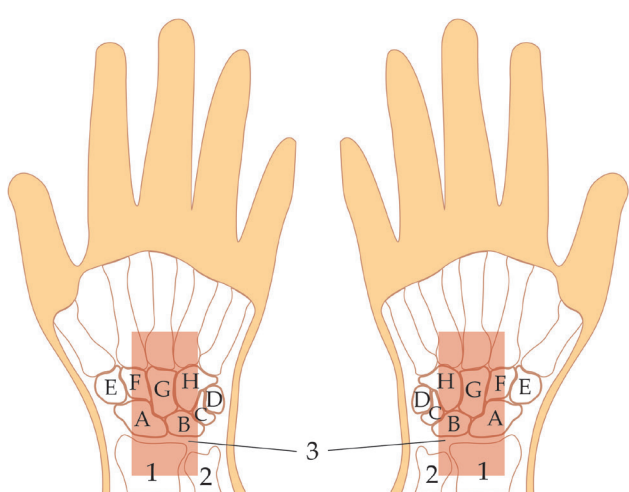


Fig. 1 Carpal bones and their locations in the hand. A: Capitate, B: Lunate, C: Triquetrum, D: Pisiform, E: Scaphoid, F: Trapezium, G: Pisiform, H: Hamate, 1: Radius, 2: Ulna; 3: carpal tunnel (based on [19])

The radius and the capitate are the two wrist bones that most commonly get fractured. The cause of both capitate and the distal radius fracture is when an individual has fallen onto an outstretched hand in order to break their fall. The capitate is required for stability and coordination. This fracture is mostly seen in young and elderly adults [1, 2]. It often occurs when the hand is breaking during a fall. It is common for capitate fractures to go unrecognized or to be misdiagnosed as a wrist sprain. Such fractures account for roughly about 60 % of all carpal fractures. The radius may be damaged in two ways: the distal radius fracture is called the "colles fracture" [1, 3]. The other fracture of the radius is the reverse of colles fracture, that is, the Smith's fracture [4, 5]. This fracture occurs when the back of the wrist is the first to break during the fall, forcing the hand under the wrist. If a distal radius fracture is left untreated, it can lead to soft tissue damage and a late development of the carpal tunnel syndrome (CTS), which is a painful condition resulting from the compression of the median nerve [1, 3, 6, 7].

The carpal tunnel is defined as the fibro-osseous tunnel on the palmar side of the wrist; the bony landmarks used to define carpal tunnel volume boundaries are variable. [8] Given that posture-related changes in tunnel volume and shape are partially contingent in individual bone motions, it is essential to consider the positions of all four bony attachments of the transverse carpal ligament. Proximal boundary definitions have included the radiocarpal joint, the distal tip of the radial styloid, the most proximal aspect of the pisiform, and the distal edge of the capitate. [1, 10, 11] Linking changes in carpal tunnel shape to the wrist bones would enable potential errors associated with volume rendering from MRI to be assessed [1, 3, 11, 12].

To be able to describe these failure phenomena, a compression mechanical testing of carpal bones is made, where on the basis of the 3D images of the intact bones and artificially damaged bones their injuries are evaluated. In the case of middle finger bones, their size permits a twist test, but in this case it is not possible because of the geometry of the carpal bones, which hinders proper gripping [1, 13–16]. The tendons which connect the carpal bones have been tested several times, because they are also vulnerable. Researchers investigated the carpal bones system as a whole, but they did not examine them separately [1, 3, 11–13]. Few literary sources were available; we could not compare the results. They show modeling rather than practical utility [15, 17–19].

In the present study, the behavior of several types of carpal bones were investigated in the case of static compression tests with high speed loading. Before and after the compression test, a 3D scanner was used to create 3D images for the determination of the geometrical properties of the investigated bones. The load and the strain were measured during the mechanical test of different types of carpal bones. The Young's moduli were calculated at an early stage of the graph with deformations between 1 and 2 % [20–22]. The goal of the present research is to create a quick and inexpensive measurement method to characterize the geometrical and mechanical properties of carpal bones. In the four preliminary experiments, bones of different geometries were examined, forming part of the carpal bones system.

2 Materials and methods

The four types of carpal bones were investigated, including capitate, scaphoid, trapezium and pisiform (Fig. 1). All 4 pieces of bones were removed from the same human cadaver within 24 hours post mortem. The bones were placed in a radio-cryoprotectant solution and cooled and stored them at 5°C until mechanical testing (max. 1 week). Before the 3D images are acquired, the bones must be cleaned from the soft tissues with medical tweezers to fit the bone into a stable bone cement base, ensuring exact placement for both geometric and mechanical measurements. After the consolidation of the medical bone cement, a GOM ATOS Core 5M 3D scanner (Gesellschaft für optische Messtechnik GmbH, Germany) was used to make 3D images of the intact bone (Fig. 2). The cross-sectional area of the initial samples was measured using 3D software (Autodesk Inventor 2018) based on 3D images.



Fig. 2 GOM ATOS Core 5M 3D scanner [23]



Fig. 3 ZWICK Z2020 tensile tester before the test

The compression test was performed at room temperature using a Zwick Z2020 (Zwick GmbH, Ulm, Germany) computer-controlled t tester (Fig. 3). The static load was defined by 700 mm/min constant crosshead displacement for bones. The high speed represented the fracture by falling down.

The compressive test was continued until complete failure, which was defined at 2 mm displacement.

Values of failure load and strain at failure were determined by the computer-controlled material testing machine. The Young's moduli were calculated using the resulting graphs and number results. The Young's moduli were calculated at an early stage of the graph with deformations between 1 and 2 % [20–22].

After the mechanical test, the 3D images of failed bones were produced with a GOM ATOS Core 5M 3D scanner. The cross-sectional area of the failure samples was not measured because the cross-sectional area did not change as bones were embedded in the bone cement. However, the failure mode and failure lines could be determined on the images. The removed bones were placed in a radio-cryoprotectant solution, and cooled and stored at 5°C until the destruction.

3 Results

In this preliminary study, four carpal bones (capitate, scaphoid, trapezium and pisiform) were investigated. 3D images about the intact bones are shown in Fig. 4(a) (capitate), Fig. 6(a) (scaphoid), Fig. 8(a) (trapezium), and Fig. 10(a) (pisiform). The measured cross-sectional areas are summarized in Table 1.

The standard force – strain diagrams for the compressive test are shown in Fig. 5 (capitate), Fig. 7 (scaphoid), Fig. 9 (trapezium), and Fig. 11 (pisiform). The measured (failure load, strain at failure) and the calculated (Young's modulus of elasticity) results are summarized in Table 2.

The 3D images of the damaged bones are shown in Fig. 4(b) (Capitate), Fig. 6(b) (Scaphoid), Fig. 8(b) (Trapezium), and Fig. 10(b) (Pisiform).

The results showed that the trapezium bone (failure load: 6507.96 N, failure stress: 16.96 N/mm²) was the strongest bone among the bones measured. It was about 12 times stronger than the weakest capitate bone (failure



(a)



(b)

Fig. 4 3D images of the capitate bone a) (left) before the compressive test (intact) b) (right) after the compressive test (failed)

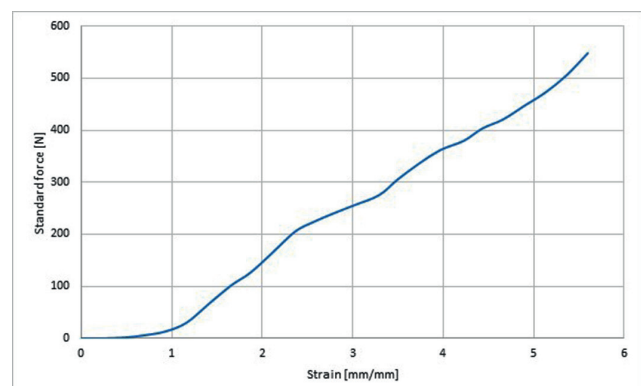


Fig. 5 Force and strain curve of capitate bone



(a)



(b)

Fig. 6 3D images of the scaphoid bone a) (left) before the compressive test (intact) b) (right) after the compressive test (failed)

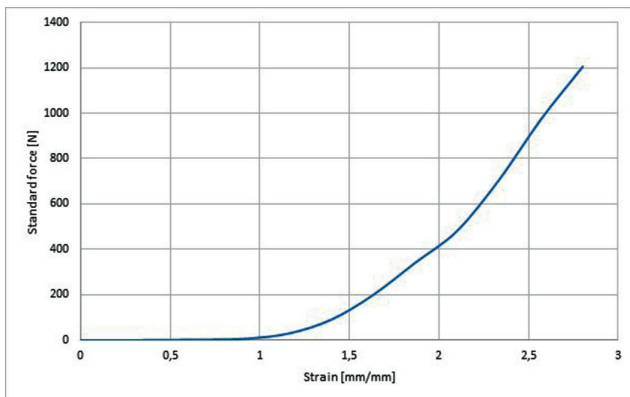


Fig. 7 Force and strain curve of scaphoid bone

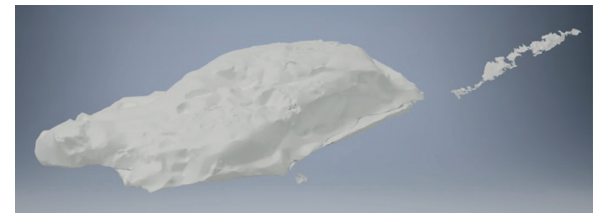
load: 548.15 N, failure stress: 1.34 N/mm^2). The Young's moduli of elasticity showed a similar tendency. The biggest deformity was measured at the pisiform bone (10.97 %). The smallest deformity was measured at the scaphoid bone (2.80 %).

4 Conclusions

The goal of the present research is to create a quickly and inexpensive measurement method to characterize the geometrical and mechanical properties of carpal bones. The resulting 3D images allow to insert bones into a finite



(a)



(b)

Fig. 8 3D images of the trapezium bone a) (left) before the compressive test (intact) b) (right) after the compressive test (failed)

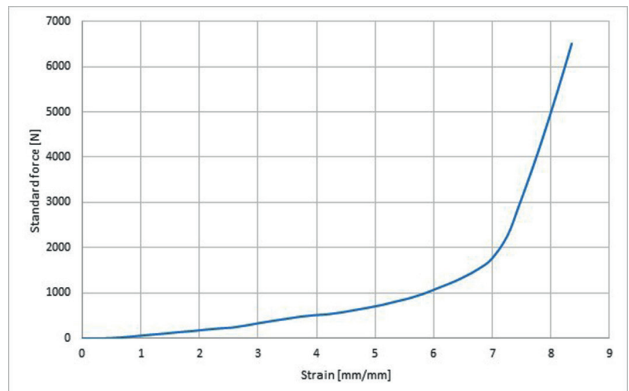


Fig. 9 Force and strain curve of trapezium bone

element program for later modeling as input geometrical data and mechanical properties. The novelty of the present research is that the mechanical test has been combined with 3D imaging.

In the examined carpal bones, a large deviation of mechanical and geometrical parameters was observed (Fig. 12). The cause of large deviation is that different carpal bones are investigated. In this preliminary study, we have defined the measurement layout, the preparation of the measurement, and the measured and calculated mechanical parameters required for the investigation of different carpal bones.

In order to compare the biomechanical behavior of the different bones, the apparent Young's modulus values were evaluated. In case of Young's moduli an almost 25-fold difference was observed between the strongest and the weakest bones (Table 1). The tendency of failure load and failure stress is similar (Table 1). This phenomenon can be explained by its location in the hand and its size. The shape



(a)



(b)

Fig. 10 3D images of the pisiform bone a) (left) before the compressive test (intact) b) (right) after the compressive test (failed)

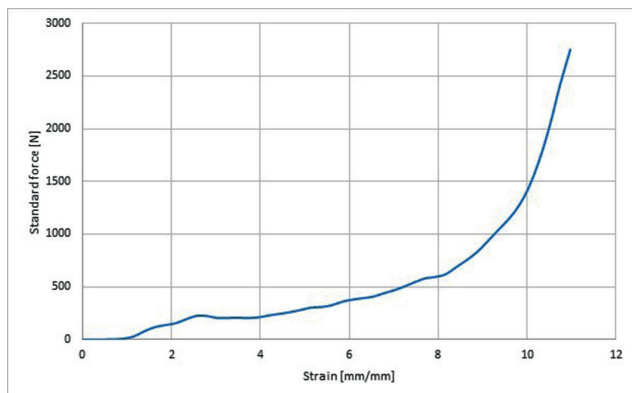


Fig. 11 Force and strain curve of pisiform bone

of the curves is also worth investigating (Fig. 12). In the case of the capitate bone, the inclination of the curve is lower than in the other cases (Fig. 12). After the maximum load there is no initial and leap failure. (Fig 12), which can be explained by the geometry of the bone. The graph of the capitate bone showed a "saw-tooth character" before the failure. This means that more and more "bone sticks of spongiosa" are failed before the maximum load (Fig. 12). It can be explained by the high volume percent of spongiosa in the capitate bone, which can be seen in Fig 4(b).

The limit of the present study is that only one sample of each capital bone was investigated. In further research,

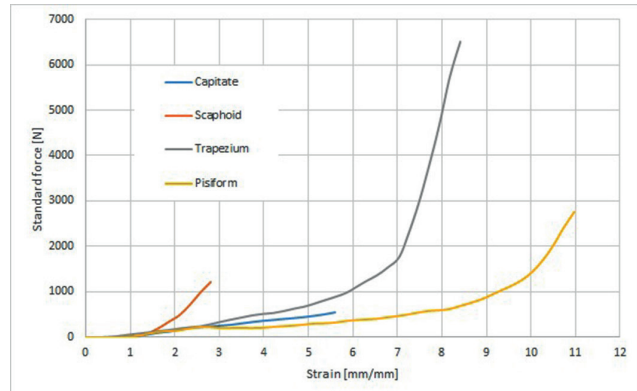


Fig. 12 The force and strain curves of all bones investigated in the present preliminary research

Table 1 Cross-sectional area values of samples

	Capitate	Scaphoid	Trapezium	Pisiform
Cross-sectional area [mm ²]	408.42	455.53	383.64	265.49

Table 2 Measured and calculated parameters of compressive test

	Capitate	Scaphoid	Trapezium	Pisiform
Failure load [N]	548.15	1204.29	6507.96	2754.03
Failure stress [N/mm ²]	1.34	2.64	16.96	10.37
Strain at failure [mm/mm]	5.61	2.80	8.36	10.97
Young's modulus of elasticity	3.61	21.82	92.09	67.17

the number of samples from each carpal bone should be increased. However, the preliminary study and its results have confirmed that the complex method is suitable for the determination of the geometrical and mechanical properties of small bones, such us carpal bones. The results of the new complex method can be used be for the modelling and simulation of the failure of carpal bones. It can be used for the 3D printing of different carpal bones.

Acknowledgement

The research reported in this paper was supported by the Higher Education Excellence Program of the Ministry of Human Capacities in the frame of Biotechnology research area of Budapest University of Technology and Economics (BME FIKP-BIO). This research was supported by The National Research, Development and Innovation Office (OTKA K 116189 and NVKP_16-1-2016-0022). The research reported in this paper has been supported by the National Research, Development and Innovation Fund (TUDFO/51757/2019-ITM, Thematic Excellence Program).

References

- [1] Khader, B. A., Towler, M. R. "Common treatments and procedures used for fractures of the distal radius and Capitate: A review", Materials Science and Engineering: C, 74, pp. 422–433, 2016.
<https://doi.org/10.1016/j.msec.2016.12.038>
- [2] Xiu, K.-H., Kim, J.-H., Li, Z.-M. "Biomechanics of the transverse carpal arch under carpal bone loading", Clinical Biomechanics, 25(8), pp. 776–780, 2010.
<https://doi.org/10.1016/j.clinbiomech.2010.05.011>
- [3] Moojen, T. M., Snel, J. G., Ritt, M. J. P. F., Venema, H. W., Kauer, J. M. G., Bos, K. E. "In vivo analysis of carpal kinematics and comparative review of the literature", The Journal of Hand Surgery, 28(1), pp. 81–87, 2003.
<https://doi.org/10.1053/jhsu.2003.50009>
- [4] Kamal, R. N., Starr, A., Akelman, E. "Carpal Kinematics and Kinetics", The Journal of Hand Surgery, 41(10), pp. 1011–1018, 2016.
<https://doi.org/10.1016/j.jhsa.2016.07.105>
- [5] Garcia-Elias, M., An, K.-N., Cooney, W. P., Linscheid, R. L., Chao, E. Y. S. "Stability of the transverse carpal arch: An experimental study", The Journal of Hand Surgery, 14(2), pp. 277–282, 1989.
[https://doi.org/10.1016/0363-5023\(89\)90021-X](https://doi.org/10.1016/0363-5023(89)90021-X)
- [6] Crisco, J., Heard, W., Rich, R., Paller, D., Wolfe, S. "The Mechanical Axes of the Wrist Are Oriented Obliquely to the Anatomical Axes", The Journal of Bone and Joint Surgery, 93(2), pp. 169–177, 2011.
<https://doi.org/10.2106/JBJS.I.01222>
- [7] Cooney, W. P., Dobyns, J. H., Linscheid, R. L. "Arthroscopy of the wrist: Anatomy and classification of carpal instability", Arthroscopy: The Journal of Arthroscopic & Related Surgery, 6(2), pp. 133–140, 1990.
[https://doi.org/10.1016/0749-8063\(90\)90014-5](https://doi.org/10.1016/0749-8063(90)90014-5)
- [8] Schuind, F., Cooney, W. P., Linscheid, R. L., An, K. N., Chao, E. Y. S. "Force and pressure transmission through the normal wrist. A theoretical two-dimensional study in the posteroanterior plane", Journal of Biomechanics, 28(5), pp. 587–589, 1995.
[https://doi.org/10.1016/0021-9290\(94\)00093-J](https://doi.org/10.1016/0021-9290(94)00093-J)
- [9] Wikipedia "Carpal bones", [online] Available at: https://en.wikipedia.org/wiki/Carpal_bones [Accessed: 13 November 2019]
- [10] Petterson, R. M., Moritomo, H., Yamaguchi, S., Mitsuyasu, H., Shah, M., Buford, W. L., Viegas, S. F. "Scaphoid anatomy and mechanics: Update and review", Operative Techniques in Orthopaedics, 13(1), pp. 2–10, 2003.
<https://doi.org/10.1053/otor.2003.36316>
- [11] Mogk, J. P. M., Keir, P. J. "The effect of landmarks and bone motion on posture-related changes in carpal tunnel volume", Clinical Biomechanics, 24(9), pp. 708–715, 2009.
<https://doi.org/10.1016/j.clinbiomech.2009.05.012>
- [12] Foumani, M., Blankevoort, L., Stekelenburg, C., Strackee, S. D., Carelsen, B., Jonges, R., Streekstra, G. J. "The effect of tendon loading on in-vitro carpal kinematics of the wrist joint", Journal of Biomechanics, 43(9), pp. 1799–1805, 2010.
<https://doi.org/10.1016/j.jbiomech.2010.02.012>
- [13] Márquez-Florez, K., Vergara-Amador, E., Gavilán-Alfonso, M., Garzón-Alvarado, D. "Load distribution on the radio-carpal joint for carpal arthrodesis", Computer Methods and Programs in Biomedicine, 127, pp. 204–215, 2016.
<https://doi.org/10.1016/j.cmpb.2015.12.023>
- [14] Crisco, J. J., Pike, S., Hulsizer-Galvin, D. L., Akelman, E., Weiss, A.-P., Wolfe, S. W. "Carpal bone postures and motions are abnormal in both wrists of patients with unilateral scapholunate interosseous ligament tears", The Journal of Hand Surgery, 28(6), pp. 926–937, 2003.
[https://doi.org/10.1016/S0363-5023\(03\)00422-2](https://doi.org/10.1016/S0363-5023(03)00422-2)
- [15] Guo, X., Fan, Y., Li, Z.-M. "Effects of dividing the transverse carpal ligament on the mechanical behavior of the carpal bones under axial compressive load: A finite element study", Medical Engineering & Physics, 31(2), pp. 188–194, 2009.
<https://doi.org/10.1016/j.medengphy.2008.08.001>
- [16] Varga, P., Schefzig, P., Unger, E., Mayr, W., Zyssset, P. K., Erhart, J. "Finite element based estimation of contact areas and pressures of the human Capitate in various functional positions of the hand", Journal of Biomechanics, 46(5), pp. 984–990, 2013.
<https://doi.org/10.1016/j.jbiomech.2012.11.053>
- [17] Gabra, J. N., Li, Z.-M. "Three-dimensional stiffness of the carpal arch", Journal of Biomechanics, 49(1), pp. 53–59, 2016.
<https://doi.org/10.1016/j.jbiomech.2015.11.005>
- [18] Varga, P., Zyssset, P. K., Schefzig, P., Unger, E., Mayr, W., Erhart, J. "A finite element analysis of two novel screw designs for Capitate waist fractures", Medical Engineering & Physics, 38(2), pp. 131–139, 2016.
<https://doi.org/10.1016/j.medengphy.2015.11.006>
- [19] University of Washington "Meet Dermestes maculatus: The Burke Museums flesh-eating volunteers", [online] Available at: <http://www.washington.edu/news/2011/01/03/meet-dermestes-maculatus-the-burke-museums-flesh-eating-volunteers/> [Accessed: 13 November 1993]
- [20] Kurutz, M., Tornyos, Á. "Numerical simulation and parameter identification of human lumbar spine segments in traction" In: Proceedings of the First Hungarian Conference on Biomechanics, Budapest, Hungary, 2004, pp. 254–263.
<https://www.researchgate.net/publication/260530824>
- [21] Kurutz, M., Varga, P., Jakab, G. "Prophylactic vertebroplasty versus kyphoplasty in osteoporosis: A comprehensive biomechanical matched-pair study by in vitro compressive testing", Medical Engineering & Physics, 65, pp. 46–56, 2019.
<https://doi.org/10.1016/j.medengphy.2019.01.004>
- [22] Kurutz, M., Jakab, G., Varga, P., Varga, P. P. "Biomechanical evaluation of vertebroplasty and kyphoplasty by uniaxial compressive test", Biomechanica Hungarica, 6(1), pp. 311–322, 2013.
<https://doi.org/10.17489/biohun/2013/1/33>
- [23] BME "3D Optikai Mérőrendszer - GOM" (3D Optical Measuring System - GOM), [online] Available at: <http://www.pt.bme.hu/gepadat.php?sorszam=154&l=a> [Accessed: 13 November 1993]